Vol. 6, No. 2, April 2022, pp. 129–136

Current Optics and Photonics

Regular Paper

Highly Birefringent Slotted-porous-core Photonic Crystal Fiber with Elliptical-hole Cladding for Terahertz Applications

Yong Soo Lee[1], Soeun Kim[2]*, and Kyunghwan Oh[1]**

[1]*Department of Physics, Yonsei University, Seoul 03722, Korea*
[2]*Integrated Optics Laboratory, Advanced Photonic Research Institute, Gwangju Institute of Science and Technology, Gwangju 61005, Korea*

(Received December 14, 2021 : revised February 7, 2022 : accepted February 21, 2022)

We propose a photonic crystal fiber (PCF) with a slotted porous core and elliptical-hole cladding, for high birefringence in the terahertz regime. Asymmetry in the guided mode is obtained mainly by using arrays of elliptical air holes in the TOPAS® polymer cladding. We investigate the tradeoff between several structural parameters and find optimized values that can have a high birefringence while satisfying the single-mode condition. The optical properties in the terahertz regime are thoroughly analyzed in numerical simulations, using a full-vector finite-element method with the perfectly-matched-layer condition. In an optimal design, the proposed photonic crystal fiber shows a high birefringence of 8.80×10^{-2} and an effective material loss of 0.07 cm^{-1} at a frequency of 1 THz, satisfying the single-mode-guidance condition at the same time. The proposed PCF would be useful for various polarization-management applications in the terahertz range.

Keywords : High birefringence, Photonic crystal fiber, Terahertz
OCIS codes : (060.2280) Fiber design and fabrication; (060.5295) Photonic crystal fibers; (260.1440) Birefringence

I. INTRODUCTION

Long-distance transmission of terahertz electromagnetic waves is a well-known technical challenge, since these waves suffer high loss in most waveguide materials [1]. Therefore, transmission of terahertz waves has been usually achieved through free space over a relatively short distance, without resorting to waveguides. Free-space transmission, however, also has an inherent problem, caused by the strong terahertz absorption of water vapor in the air, which can hardly be under fine control. Due to the high potential of THz applications, such as molecular sensing and spectroscopy [2], noninvasive medical imaging [3], modulators [4], and recently 5G wireless communication [5], there have been continuous efforts to overcome the technical challenges of terahertz wave transmission.

As successfully proven in the optical frequency range, optical fiber/waveguide technologies have been attempted in the terahertz range, including circular and rectangular metallic pipe waveguides [6], parallel-plate waveguides [7], single-crystal sapphire fiber [8], metallic wire waveguides [9], and photonic crystal fibers (PCFs) [10–16]. Among them, PCF has incessantly attracted a lot of research interest because it can control the guiding properties flexibly, to a level that cannot be achieved by other means. In recent sophisticated terahertz applications such as hyperfine sensing, high-fidelity communication, and terahertz heterodyne detection, precise control of the polarization state of the terahertz wave has been in high demand. This can be accomplished by using a highly birefringent terahertz fiber.

*Corresponding author: sekim@gist.ac.kr, ORCID 0000-0001-5138-4604
**Corresponding author: koh@yonsei.ac.kr, ORCID 0000-0003-2544-0216

Color versions of one or more of the figures in this paper are available online.

This is an Open Access article distributed under the terms of the Creative Commons Attribution Non-Commercial License (http://creativecommons.org/licenses/by-nc/4.0/) which permits unrestricted non-commercial use, distribution, and reproduction in any medium, provided the original work is properly cited.

Copyright © 2022 Current Optics and Photonics

pISSN: 2508-7266 / eISSN: 2508-7274 https://doi.org/10.3807/COPP.2022.6.2.129

The birefringence in the terahertz PCF can be increased by increasing the anisotropy of the waveguide structure, such as changing the size of the air hole near the core region or the cladding, deforming the air hole's shape, or deforming the core's shape [17]. In terahertz PCFs, birefringence greater than 10^{-2} has been recently reported in asymmetric cores composed of elliptical air holes around the core, but the loss was not sufficiently low [18]. In conventional PCF, the central defect serves as the core of the waveguide [19] and the material loss of the defect significantly increases the total attenuation of the guided modes. To reduce the material loss in the core of terahertz PCFs, a porous core has been proposed, and it has provided not only low attenuation but also lower chromatic dispersion [13–16, 20].

In this study, we propose a novel PCF waveguide structure made of cyclic olefin copolymer (COC) [21] and consisting of a slotted porous core plus cladding with elliptical air holes. The elliptical core has several slotted air holes along the major-axis direction, to increase the anisotropy of the PCF, and the air region within the slots contributes to lowering the effective material loss (EML). Waveguide parameters and their roles in the optical characteristics such as the birefringence, EML, and dispersion properties are analyzed, and tradeoffs between them are investigated, to satisfy the single-mode condition in the interesting frequency band below 1 THz. As a result, the proposed fiber achieves a high birefringence of 8.80×10^{-2} and a very low EML of 0.07 cm^{-1} at 1 THz, while simultaneously satisfying the single-mode condition. By calculating the cladding mode in the frequency range of 0.7−1.1 THz, the cutoff of the higher-order modes by the cladding mode is confirmed. This also guarantees that the proposed PCF is only relevant for the fundamental mode.

II. DESIGN METHODOLOGY

The cross section of the proposed PCF is shown in Fig. 1. The COC, a commercial product known as TOPAS (TOPAS Advanced Polymers, MI, USA) is considered an optimal plastic material for terahertz PCFs [21], due to its low material loss of 0.2 cm^{-1} at 1 THz, as well as its flexible manufacturing capability. TOPAS has a constant refractive index of $n = 1.53$ in the range of 0.1 to 2 THz. In this study, the proposed PCF is based on TOPAS and the holes and slots are filled with air.

The elliptical holes (with major axis a and minor axis b) in the cladding are arranged in an isosceles triangular lattice with hole-to-hole period of Λ. In the cladding, the ellipticity ratio is simply defined as $\eta = a/b$. The core defect has the same ellipticity ratio η, and we define the horizontal distance between the elliptical air holes located in the first layer of the cladding as the core size D_{core}, as shown in the inset of Fig. 1. Within the core are embedded five air slots of height h that is scaled to $1.1\eta D_{core}$ (for the center slot), $0.81\eta D_{core}$ (two inner slots), or $0.7\eta D_{core}$ (two outer slots). The slot width w is a key parameter to control the core porosity, along with h and the pitch of the slots Λ_c. Core porosity is defined as the ratio of the air-slots area to the cross-sectional area of the core [22]. It is advantageous for the porous core to have a sufficiently high air filling fraction $2b/\Lambda$ of the cladding, because then the mode confinement is weaker than that of a solid core [20]. Enhancing the mode confinement also helps to reduce confinement loss and increase birefringence [23]. We set the air filling fraction to be 0.95, the maximum practical value achievable in the proposed structure.

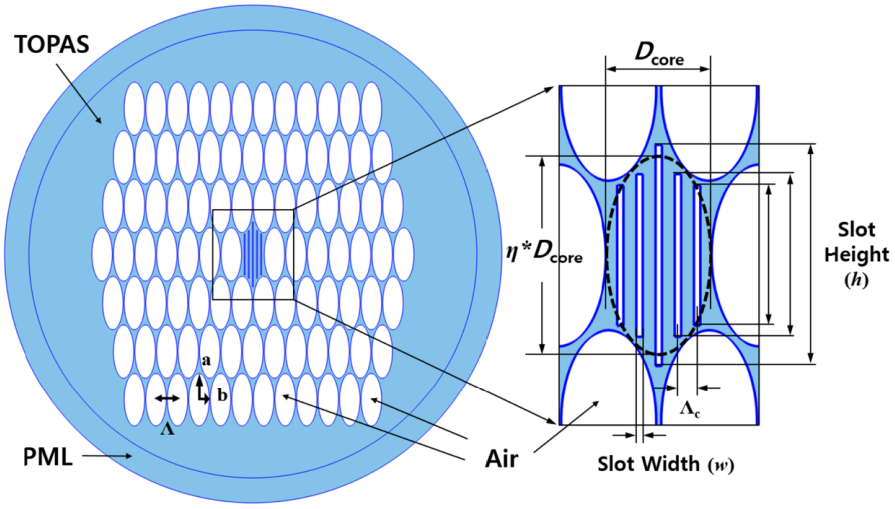

FIG. 1. Transverse cross section of the proposed photonic crystal fiber (PCF) design, and the extended view of the slotted porous core.

III. NUMERICAL ANALYSIS AND DISCUSSION

To analyze the optical properties of the proposed PCF, we use a full-vectorial finite-element-method (FEM) package (COMSOL Multiphysics v. 5.4; COMSOL Inc., MA, USA) and the perfectly-matched-layer (PML) boundary condition, where 10% of the outer cladding radius was assumed to be the absorbing boundary, reducing the surrounding environment's effect.

The electric field distributions of the fundamental guided modes are shown for (a) *x*- and (b) *y*-polarized fundamental modes in Fig. 2. Here the core porosity is 22%, D_{core} = 121 μm and η = 2.0 at a frequency of 1 THz. Both polarizations of the fundamental mode are well confined in the porous core region, and the *x*-polarized mode is selectively confined in the air slots. Due to this disparity in the polarization direction of the guided mode, we can expect a high birefringence. Also, since the *x*-polarized mode is mostly confined to the air slots and has less interaction with the material, we can expect lower EML than for the *y*-polarized mode.

Note that the parameters used in Fig. 2 are optimized to consider the tradeoff between birefringence and the single-mode condition. The birefringence is calculated using the standard definition [19]

$$B = \left| n_{\text{eff}}^{x} - n_{\text{eff}}^{y} \right|, \tag{1}$$

where n^{x}_{eff} and n^{y}_{eff} are the effective refractive indices of the *x*- and *y*-polarized fundamental modes respectively. The single-mode condition is checked by comparing the effective indices of the core modes and the space-filling mode in the cladding [24]. In the cladding of the proposed PCF, in which elliptical air holes with different lattice constants are arranged depending on the direction, it is not easy to determine whether the single-mode condition is satisfied with the *V* parameter. We analyze the single-mode guidance conditions by varying waveguide parameters (the ellipticity η, the core porosity, and D_{core}), and the results are summarized in Figs. 3–5.

As we vary the ellipticity ratio η, we investigate its impact on optical properties, and the results are summarized in Fig. 3. The remaining two parameters, D_{core} and porosity, are fixed at 121 μm and 22% respectively. Figure 3(a) shows that the birefringence increases as η increases. The red and blue lines indicate the *y*- and *x*-polarized fundamental modes respectively. As shown in Fig. 2, since the *x*-polarized fundamental mode is mostly confined within the air slot with a low refractive index, it shows a relatively low effective mode index. The black and grey lines indicate the cladding mode and 2nd higher mode, respectively. The curve with symbols indicates the birefringence which is the magnitude of the difference between the indices of the *y*- and *x*-polarized fundamental modes. The filled symbols indicate the birefringence when the fiber satisfies the single-mode condition, while the empty symbols indicate the birefringence when it does not. Note that the birefringence increases with η, but an elliptical core that is too elongated in the major axis (with a large η) makes it difficult to satisfy the single-mode condition. With D_{core} = 121 μm and core poros-

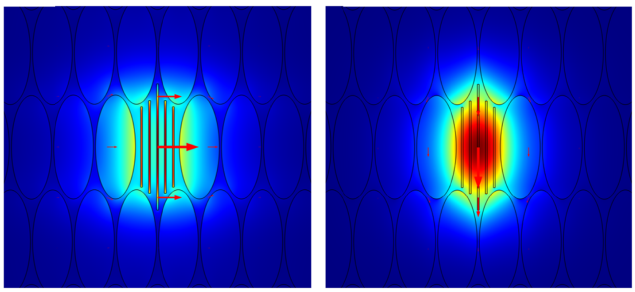

(a) (b)

FIG. 2. Electric field distribution of the fundamental mode: (a) *x*-polarization and (b) *y*-polarization, with D_{core} = 121 μm, η = 2.6, and core porosity of 22% at a frequency of 1 THz.

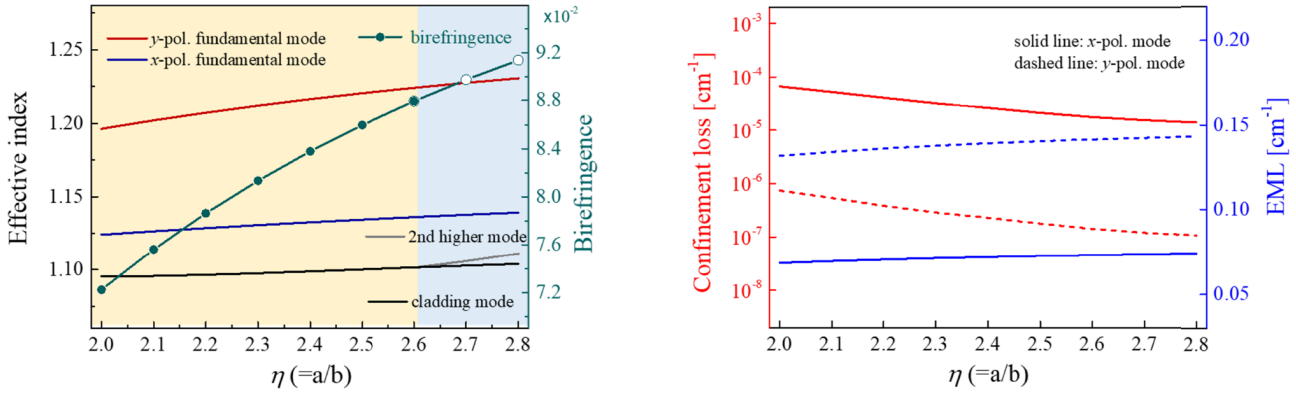

(a) (b)

FIG. 3. Impact of varying η: (a) single-mode guidance and birefringence and (b) losses at a frequency of 1 THz as a function of η, with D_{core} = 121 μm and core porosity of 22%.

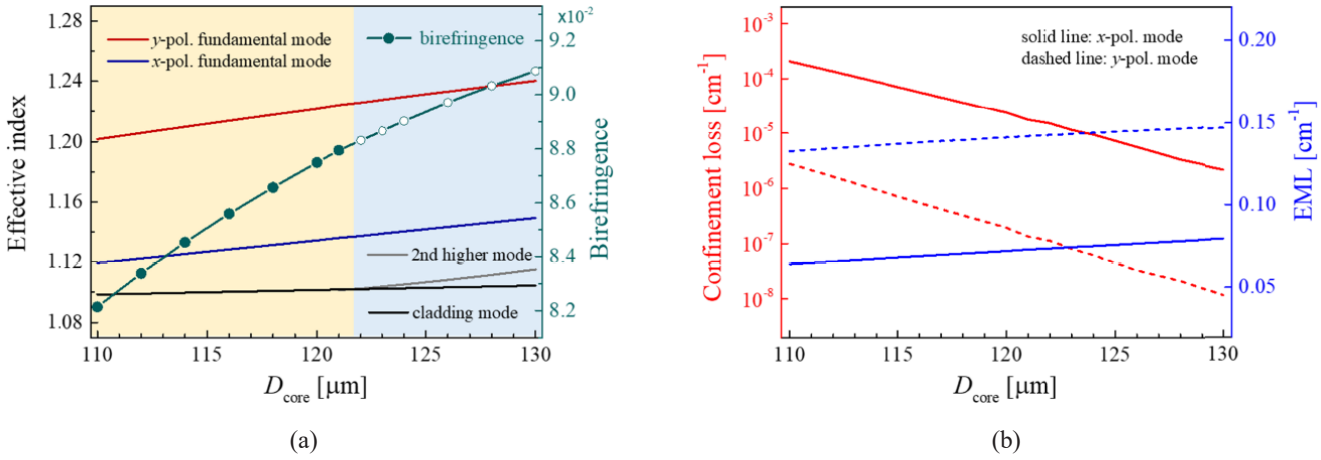

(a) (b)

FIG. 4. Impact of varying D_{core}: (a) single-mode guidance and birefringence and (b) losses at a frequency of 1 THz as a function of D_{core}, with η = 2.6 and core porosity of 22%.

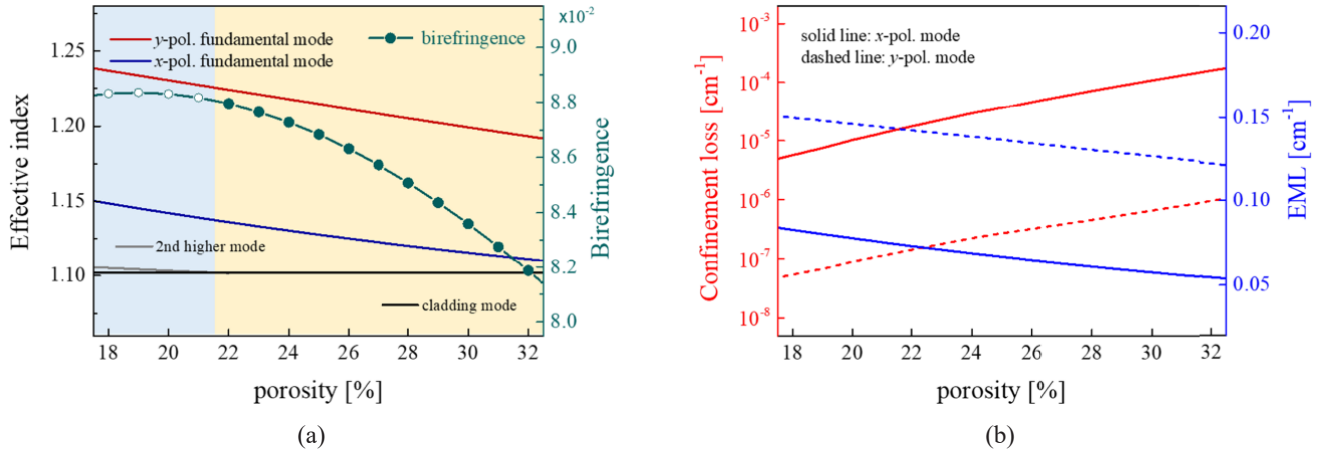

(a) (b)

FIG. 5. Impact of varying porosity: (a) single-mode guidance and birefringence and (b) losses at a frequency of 1 THz as a function of porosity, with D_{core} = 121 μm and η = 2.6.

ity of 22%, when η = 2.6 the 2nd higher mode is cut off by the cladding mode, and the proposed PCF has the largest birefringence while satisfying the single-mode condition. Fig. 3(b) shows the change in loss of the proposed THz PCF as a function of η. The confinement loss L_c originates from the finite number of air-hole rings in the cladding [25] and is expressed as

$$L_c = \left(\frac{4\pi f}{c}\right)\mathrm{Im}\left(n_{\mathrm{eff}}\right),\ \mathrm{cm}^{-1}, \tag{2}$$

where Im(n_{eff}) represents the imaginary part of the complex effective index of the guided mode, f is the operating frequency, and c is the speed of light. The EML of the fiber is calculated by using the following equation [16]:

$$\alpha_{\mathrm{eff}} = \sqrt{\frac{\varepsilon_0}{\mu_0}}\left(\frac{\int_{\mathrm{mat}} n_{\mathrm{mat}}\left|E\right|^2 \alpha_{\mathrm{mat}} dA}{\left|\int_{\mathrm{all}} S_z dA\right|}\right), \tag{3}$$

where ε_0 and μ_0 are the permittivity and permeability of the vacuum respectively. The Poynting vector S_z, which represents the magnitude of the electromagnetic power flow along the axial direction, is defined as $S_z = 1/2 \cdot \mathrm{Re}\left(\vec{E} \times \vec{H}^*\right)\hat{z}$, where E is the electric field and H^* is the complex conjugate of the magnetic field. In Fig. 3(b), the red and blue lines indicate the confinement loss L_c and effective material loss (EML) respectively. The solid and dashed lines indicate the x- and y-polarization modes respectively. As η increases, L_c monotonically decreases but EML increases. As shown in Fig. 2(a), the x-polarized mode, which is mostly confined to the air slot, has a much lower EML than the y-polarized mode, while the L_c of the x-polarized mode is relatively high. As can be seen in Fig. 3(b), EML is the dominant factor in determining THz propagation in the proposed PCF, because L_c is much smaller than the EML and has little effect on total loss. In the PCF with the proposed structure, the largest η that satisfies the single-mode condition is 2.6, which is an optimal value.

The dependence of the optical characteristics on D_{core}

is summarized in Fig. 4. With η = 2.6 and core porosity of 22%, both birefringence and EML show a monotonic increase with D_{core}, in Figs. 4(a) and 4(b) respectively. In contrast, the confinement loss monotonically decreases. When D_{core} is smaller than 122 μm, it can maintain fundamental core modes. The optimal core diameter is found to be D_{core} = 121 μm, considering both the single-mode condition and high birefringence.

Impact of the core porosity on the optical properties of the proposed fiber is analyzed in Fig. 5. When the porosity is 19% the proposed PCF has maximum birefringence, but does not satisfy the single-mode condition. When the porosity begins to increase above 19%, the birefringence and EML monotonically decrease, as shown in Figs. 5(a) and Fig. 5(b) respectively, while the confinement loss monotonically increases, as in Fig. 5(b). The optimal core porosity is found to be 22%, considering both the single-mode condition and high birefringence.

Considering single-mode guidance, high birefringence, and losses, we find D_{core} = 121 μm, η = 2.0, and porosity = 22% to be the optimal values to achieve maximum birefringence. The proposed PCF has a high birefringence of 0.088 at 1 THz. Figure 6 shows the optical properties of the proposed PCF with optimized parameters. Figure 6(a) indicates the change of effective index and birefringence according to changing frequency. The blue, black, and grey lines indicate the effective indices of the fundamental modes, cladding mode, and 2nd higher mode respectively, and the solid and dashed lines indicate the *x*- and *y*-polarization modes respectively. The line with symbols indicates the birefringence; filled symbols show the birefringence when the single-mode condition is satisfied, and empty symbols when not. Below 1 THz, the proposed PCF with optimized parameters satisfies the single-mode condition. At 1 THz, satisfying the single-mode condition, it has the largest birefringence value of 0.088, and the birefringence decreases with frequency. It is further noteworthy that below 0.7 THz the *x*-polarized mode of the proposed fiber is cut off by the cladding mode, so below 0.7 THz the proposed fiber can operate as single-polarization– single-mode for short-length applications, or as long as the transmittance is guaranteed. Figure 6(b) shows L_c and EML (indicated by red and blue lines) as a function of frequency. For EML, the *x*-polarized mode (confined to the air slot) has a smaller value than the *y*-polarized mode, and the EML increases with frequency for both modes. The *x*-polarized mode of the proposed PCF has a low EML of 0.07 cm^{-1}, which is much smaller than the bulk material loss of COC at 1 THz. However, in the *x*-

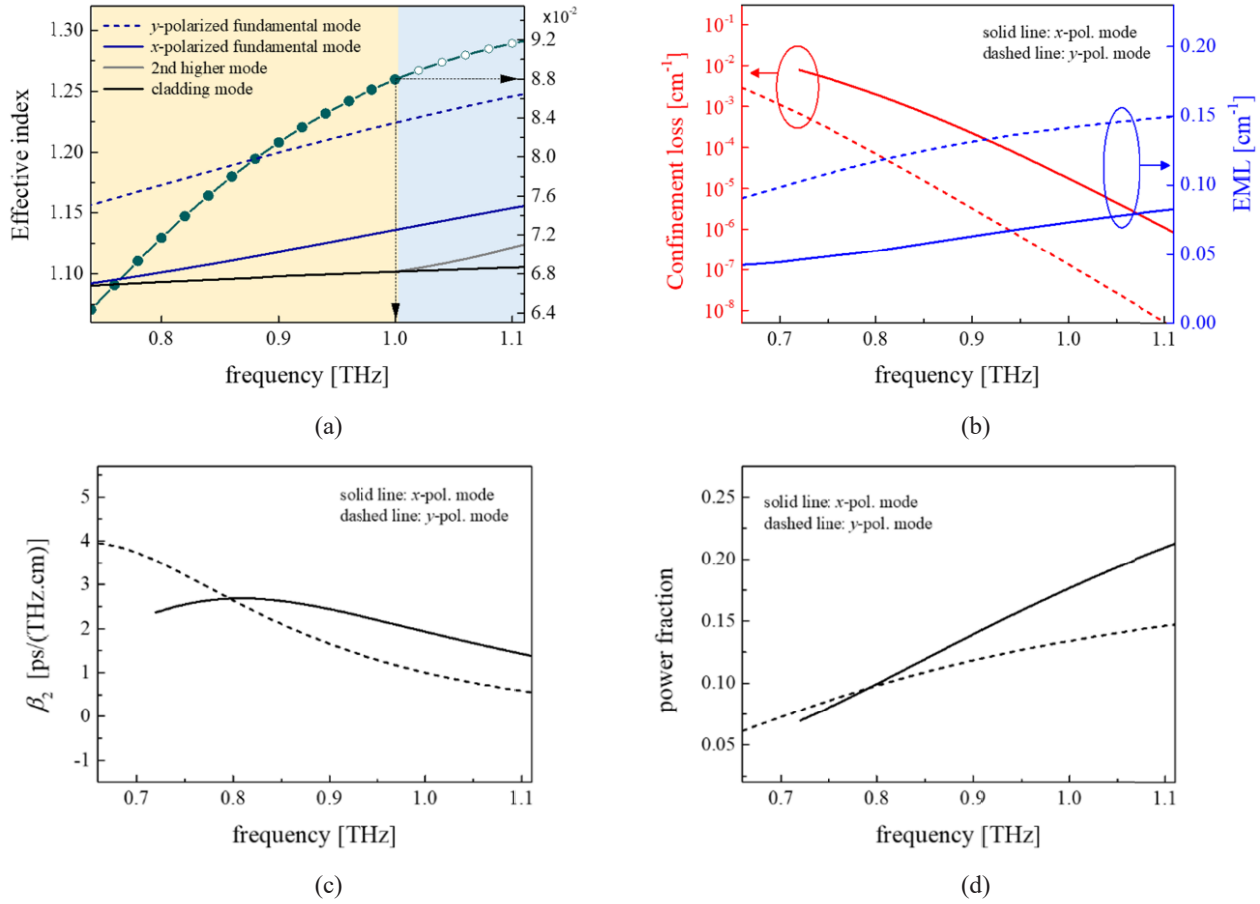

FIG. 6. Optical properties of the proposed PCF with optimized parameters D_{core} = 121 μm, η = 2.6, and porosity = 22%: (a) single-mode guidance and birefringence, (b) confinement loss and EML, (c) β_2, and (d) power fraction.

polarized mode the confinement loss gradually increases as the cutoff frequency is approached, and the confinement loss becomes non-negligible. Figure 6(c) depicts the dispersion profile for both *x*- and *y*-polarized modes as a function of frequency. The chromatic dispersion is a significant parameter for a waveguide; dispersion should be kept as low as possible to avoid induced pulse width expansion, which limits the performance of the propagating signal. One interesting feature of COC is its constant refractive index over a wide band (0.1–1.6 THz), which makes material dispersion very negligible. Thus we are mainly concerned with the waveguide dispersion of the proposed PCF, which can be calculated as [16]

$$\beta_2 = \frac{2}{c}\frac{dn_{\text{eff}}}{d\omega} + \frac{\omega}{c}\frac{d^2 n_{\text{eff}}}{d\omega^2},\ \text{ps/(THz}\cdot\text{cm)}, \tag{4}$$

where the angular center frequency is $\omega = 2\pi f$. The dispersion value for the *x*-polarized mode is higher than that for *y*-polarized mode. However, the propose PCF has low dispersion values of 1.93 ps/(THz cm) and 1.00 ps/(THz cm) at 1 THz for the *x*- and *y*-polarized modes respectively, and the *x*-polarized modeshows a flattened dispersion with low variation of 2.15 ± 0.22 ps/(THz cm), from 0.72 THz to 1 THz. Figure 6(d) shows the power fraction in the air slots, which is calculated from the following expression [16]:

$$\text{Fraction of Power} = \frac{\int_X S_z dA}{\int_{\text{all}} S_z dA}, \tag{5}$$

where the integration of the denominator is performed for the entire area and the numerator for the area of interest (denoted by *X*). The power fraction is calculated only for the area covered by the core air slots, because the major objective is engaging maximum power in the rectangular slots, to obtain extremely high birefringence. Also, the more power that flows through the core air-slot region, the better the loss profile for a particular design. The power in the air slots is 18% of the total power through the waveguide, for the *x*-polarization mode at 1 THz.

Table 1 shows the optical-guidance properties of the proposed PCF compared to those for some other terahertz waveguides with porous cores. For the proposed fiber, an asymmetric core and a cladding with an isosceles triangular lattice composed of elliptical air holes are designed to achieve high birefringence, and rectangular air slots are embedded in the core for enhanced birefringence and low EML. Note that the proposed fiber with optimized parameters simultaneously satisfies the single-mode condition, using the space-filling method. The proposed PCF birefringence using an elliptical air hole in the cladding and an elliptical core with air slots has high birefringence, compared to previously reported THz waveguides. In addition, the proposed fiber can operate as single-polarization– single-mode, as one polarization mode is cut off by the cladding mode, and it can provide excellent characteristics for terahertz applications, with its flattened dispersion and low loss.

The proposed polymer microstructure contains slot-shaped holes in the core and an isosceles triangular lattice with elliptical air holes in the cladding. These different arrangements of air holes should be fabricated using separate manufacturing methods. Fortunately, due to technological advancements the difficulties of fabricating a PCF with different shapes have diminished. For example, structures like a kagome lattice have been formed using a stack-and-draw technique, as discussed in [26], but this method is limited to either a circular or honeycomb shape, in addition to the kagome structure. Another method called preform

TABLE 1. Comparison with reported other photonic crystal fibers (PCFs)

Reference	Structure	*f* [THz]	Porosity (%)	*B*	EML	Operation mode
[10]	Hexagonal lattice structure Circle air holes porous core	0.85	-	0.033	0.43 dB/cm	single mode
[11]	Hexagonal lattice structure Circular air holes porous core	1	-	0.045	0.08 cm^{-1}	-
[12]	Spiral rings structure Circular air holes porous core	1	-	0.0483	0.085 cm^{-1}	-
[13]	Hexagonal lattice structure Elliptical air holes porous core	1.2	-	0.074	0.08 cm^{-1}	-
[14]	Hexagonal lattice structure Elliptical air holes porous core	1.3	42	0.08	0.03 cm^{-1}	-
[15]	Hexagonal lattice structure Elliptical air holes porous core	1	50	0.086	0.05 cm^{-1}	single mode
[16]	Circular structure Elliptical air holes porous core	1.2	-	0.051	0.07 cm^{-1}	single mode
Proposed PCF	Isosceles triangular lattice Slotted porous core	1	22	0.088	0.07 cm^{-1}	single mode

drilling is mostly restricted to a small number of holes, and can produce only circular shapes. Another popular method is sol-gel casting, which is relatively less precise and more appropriate for fibers with extremely high porosity [27]. However, these methods are difficult for making a core that includes air slots as we have designed. In terahertz applications, the fabrication of microstructured polymer optical fibers (MOPs) has been reported [28], and fiber-drawing studies using preforms made with 3D printers have also been reported [29]. A more generalized method called the extrusion technique, as discussed in [30], is available and provides the design freedom to fabricate noncircular air holes in microstructured fibers. This technique is well suited for making elliptical cores with slotted air holes, as well as elliptical air holes in cladding.

IV. CONCLUSION

A slotted-porous-core PCF with a cladding structure of an isosceles triangular lattice using elliptical holes has been proposed, to achieve high birefringence. For optimized waveguide parameters, the proposed PCF provides a very high birefringence of 0.088 and single-mode operation. In addition, the PCF exhibits a negligible confinement loss of 10^{-4} cm^{-1} and has a low effective material loss of 0.07 cm^{-1} at 1 THz. The structure of the proposed PCF is expected to be fabricated using the extrusion technique, and will play an important role in potential applications such as sensing, terahertz communication systems, and polarization-preserving fibers.

FUNDING

National Research Foundation of Korea (NRF 2018R1D-1A1B07049349); National Research Foundation of Korea (NRF 2019R1A2C2011293).

DISCLOSURES

The authors declare no conflicts of interest.

DATA AVAILABILITY

Data underlying the results presented in this paper are not publicly available at the time of publication, which may be obtained from the authors upon reasonable request.

REFERENCES

1. H. Han, H. Park, M. Cho, and J. Kim, "Terahertz pulse propagation in a plastic photonic crystal fiber," Appl. Phys. Lett. **80**, 2634–2636 (2002).
2. S. J. Oh, Y. Hong, K.-Y. Jeong, I. Maeng, J.-S. Suh, J. Yang, and Y.-M. Huh, "Characterization of proton-irradiated polyaniline nanoparticles using terahertz thermal spectroscopy," Crystals **11**, 765 (2021).
3. S.-H. Lee, S. Shin, Y. Roh, S. J. Oh, S. H. Lee, H. S. Song, Y.-S. Ryu, Y. K. Kim, and M. Seo, "Label-free brain tissue imaging using large-area terahertz metamaterials," Biosens. Bioelectron. **170**, 112663 (2020).
4. G. Lee, I. Maeng, C. Kang, M.-K. Oh, and C.-S. Kee, "Strong polarization-dependent terahertz modulation of aligned Ag nanowires on Si substrate," Opt. Express **26**, 13677–13685 (2018).
5. T. Yilmaz and O. B. Akan, "On the use of low terahertz band for 5G indoor mobile networks," Comput. Electr. Eng. **48**, 164–173 (2015).
6. M. D'Auria, W. J. Otter, J. Hazell, B. T. W. Gillatt, C. Long-Collins, N. M. Ridler, and S. Lucyszyn, "3-D printed metal-pipe rectangular waveguides," IEEE Trans. Compon. Packag. Manuf. Technol. **5**, 1339–1349 (2015).
7. R. Kaur, M. Islam, P. C. Agarwal, S. Kaur, and G. Kumar, "Terahertz surface plasmons propagation in semiconducting parallel plates waveguide configuration," Europhys. Lett. **134**, 38002 (2021).
8. G. M. Katyba, K. I. Zaytsev, N. V. Chernomyrdin, I. A. Shikunova, G. A. Komandin, V. B. Anzin, S. P. Lebedev, I. E. Spektor, V. E. Karasik, S. O. Yurchenko, I. V. Reshetov, V. N. Kurlov, and M. Skorobogatiy, "Sapphire photonic crystal waveguides for terahertz sensing in aggressive environments," Adv. Opt. Mater. **6**, 1800573 (2018).
9. K. Wang and D. M. Mittleman, "Metal wires for terahertz wave guiding," Nature **432**, 376–379 (2004).
10. G. K. M. Hasanuzzaman, S. Rana, and M. S. Habib, "A novel low loss, highly birefringent photonic crystal fiber in THz regime," IEEE Photon. Technol. Lett. **28**, 899–902 (2016).
11. R. Islam, Md. S. Habib, G. K. M. Hasanuzzaman, S. Rana, and M.d. A. Sadath, "Novel porous fiber based on dual-asymmetry for low-loss polarization maintaining THz wave guidance," Opt. Lett. **41**, 440–443 (2016).
12. Md. R. Hasan, Md. S. Anower, Md. A. Islam, and S. M. A. Razzak, "Polarization-maintaining low-loss porous-core spiral photonic crystal fiber for terahertz wave guidance," Appl. Opt. **55**, 4145–4152 (2016).
13. Y. Zhang, L. Xue, D. Qiao, and Z. Guang, "Porous photonic-crystal fiber with near-zero ultra-flattened dispersion and high birefringence for polarization-maintaining terahertz transmission," Optik **207**, 163817 (2020).
14. I. K. Yakasai, P. E. Abas, H. Syhaimi, and F. Begum, "Low loss and highly birefringent photonic crystal fibre for terahertz applications," Optik **206**, 164321 (2020).
15. J. Sultana, Md. S. Islam, M. Faisal, M. R. Islam, B. W.-H. Ng, H. Ebendorff-Heidepriem, and D. Abbott, "Highly birefringent elliptical core photonic crystal fiber for terahertz application," Opt. Commun. **407**, 92–96 (2018).
16. M. A. Habib and M. S. Anower, "Design and numerical analysis of highly birefringent single mode fiber in THz regime," Opt. Fiber Technol. **47**, 197–203 (2019).
17. M. Cho, J. Kim, H. Park, Y. Han, K. Moon, E. Jung, and H. Han, "Highly birefringent terahertz polarization maintaining plastic photonic crystal fibers," Opt. Express **16**, 7–12 (2008).
18. S. Li, H. Liu, N. Huang, and Q. Sun, "Broadband high bire-

fringence and low dispersion terahertz photonic crystal fiber," J. Opt. **16**, 105102 (2014).
19. K. Oh and U.-C. Paek, *Silica Optical Fiber Technology for Devices and Components: Design Fabrication and International Standards*, (Wiley, USA. 2012).
20. S. Atakaramians, S. Afshar V., T. M. Monro, and D. Abbott, "Terahertz dielectric waveguides," Adv. Opt. Photonics **5**, 169–215 (2013).
21. K. Nielsen, H. K. Rasmussen, A. J. L. Adam, P. C. M. Planken, O. Bang, and P. U. Jepsen, "Bendable, low-loss Topas fibers for the terahertz frequency range," Opt. Express **17**, 8592–8601 (2009).
22. S. F. Kaijage, Z. Ouyang, and X. Jin, "Porous-core photonic crystal fiber for low loss terahertz wave guiding," IEEE Photonics Technol. Lett. **25**, 1454–1457 (2013).
23. Y. S. Lee, C. G. Lee, Y. Jung, and S. Kim, "Diamond unit cell photonic crystal fiber with high birefringence and low confinement loss based on circular air holes," Appl. Opt. **54**, 6140–6145 (2015).
24. M. Midrio, M. P. Singh, and C. G. Someda, "The space filling mode of holey fibers: an analytical vectorial solution," J. Lightwave Technol. **18**, 1031–1037 (2000).
25. Y. S. Lee, H. Choi, B. Kim, C. Kang, I. Maeng, S. J. Oh, S. Kim, and K. Oh, "Low-loss polytetrafluoroethylene hexagonal porous fiber for terahertz pulse transmission in the 6g mobile communication window," IEEE Trans. Microw. Theory Tech. **69**, 4623–4630 (2021).
26. A. Argyros and J. Pla, "Hollow-core polymer fibres with a kagome lattice: potential for transmission in the infrared," Opt. Express **15**, 7713–7719 (2007).
27. R. T. Bise and D. J. Trevor, "Sol-gel derived microstructured fiber: fabrication and characterization," in Optical Fiber Communications Conference-OFC (Optica Publishing Group, 2005), paper OWL6.
28. M. A. van Eijkelenborg, M. C. J. Large, A. Argyros, J. Zagari, S. Manos, N. A. Issa, I. Bassett, S. Fleming, R. C. McPhedran, C. M. de Sterke, and N. A. P. Nicorovici, "Microstructured polymer optical fibre," Opt. Express **9**, 319–327 (2001).
29. L. D. van Putten, J. Gorecki, E. N. Fokoua, V. Apostolopoulos, and F. Poletti, "3D-printed polymer antiresonant waveguides for short-reach terahertz applications," Appl. Opt. **57**, 3953–3958 (2018).
30. K. M. Kiang, K. Frampton, T. M. Monro, R. Moore, J. Tucknott, D. W. Hewak, D. J. Richardson, and H. N. Rutt, "Extruded single-mode non-silica glass holey optical fibers," Electron. Lett. **38**, 546–547 (2002).